Supplementary Material

Lifting the Veil: pyrogeographic manipulation and the leveraging of environmental change by people across the Vale of Belvoir, Tasmania, Australia.

Michael-Shawn Fletcher[*1,2], Anthony Romano[1], Scott Nichols[3], William Henriquez Gonzalez[1], Michela Mariani[4], Diana Jaganjac[5], Andry Sculthorpe[6]

1 School of Geography, Earth and Atmospheric Sciences, The University of Melbourne, Carlton, Australia;

2 Australian Research Council Centre of Excellence for Indigenous Environmental Histories and Futures, James Cook University, QLD, Australia.

3 School of Plant Sciences, University of Tasmania, Tasmania, Australia.

4 School of Geography, University of Nottingham, Nottingham, Nottinghamshire, UK.

5 Birkbeck, University of London, London, UK.

6 Tasmanian Aboriginal Centre, Hobart, TAS, Australia.

***Correspondence:**

Michael-Shawn Fletcher michael.fletcher@unimelb.edu.au.

Table S1: Details of iButton data loggers installed across the Vale of Belvoir. Includes descriptions and GPS coordinates of each location and the data collection status of each logger after 171 days of deployment. P values represent results of two-sample t-tests performed on data recovered from paired loggers from the same site.

Logger no.	Shield	Data recovery	Location	Coordinates	p value (temperature)	p value (humidity)
L004	No shield	Failed	25 m inside southeast facing forest	41° 31' 30.4" S 145° 53' 15.6" E	> 0.05	< 0.05
L012	Umbrella shield	Successful				
L014	Flat shield	Successful				
S-Trap016	Shield – seed trap	Failed			< 0.05	< 0.05
S-Trap015	No shield – seed trap	Successful				
S-Trap017	Deeper inside forest – seed trap	Successful				
E005	Small, flat shield	Failed	Eastern edge of Vale, 35 m toward	41° 33' 03.7" S 145° 53' 18.9" E		
E007	No shield	Failed				

			centre of marsupial grazing patch					
L002	Shield	Failed	Grassland, 25 m from forest edge on western edge of Vale	41° 31’ 31.7” S 145° 53’ 16.4” E				
L006	No shield	Failed						
E001	Small shield	Successful	35 m inside west facing forest	41° 33’ 03.9” S 145° 53’ 21.4” E	> 0.05	> 0.05	< 0.05	> 0.05
E013	No shield	Successful			> 0.05		< 0.05	
E009	Small umbrella shield	Successful						
W019	Large shield	Failed	20 m within grassland adjacent to south-southeastern facing forest	41° 30’ 55.9” S 145° 54’ 14.0” E				
W020	No shield	Failed						
W008	Large shield	Failed		41° 30’ 55.8” S				

W011	No shield	Successful	20 m inside south-southeastern facing forest	145° 54’ 12.4” E		
W003	Small umbrella shield	Successful			> 0.05	< 0.05
W018	Large shield	Successful	Within Richea heathland	41° 30’ 55.1” S 145° 54’ 14.9” E		
W010	No shield	Failed				

Figure S1: Summary plots of undated sediment cores used in this study, see figure 1b in main text for site locations, red dashed line indicates 1850-1890's fire documented in Marsden-Smedley (1998)

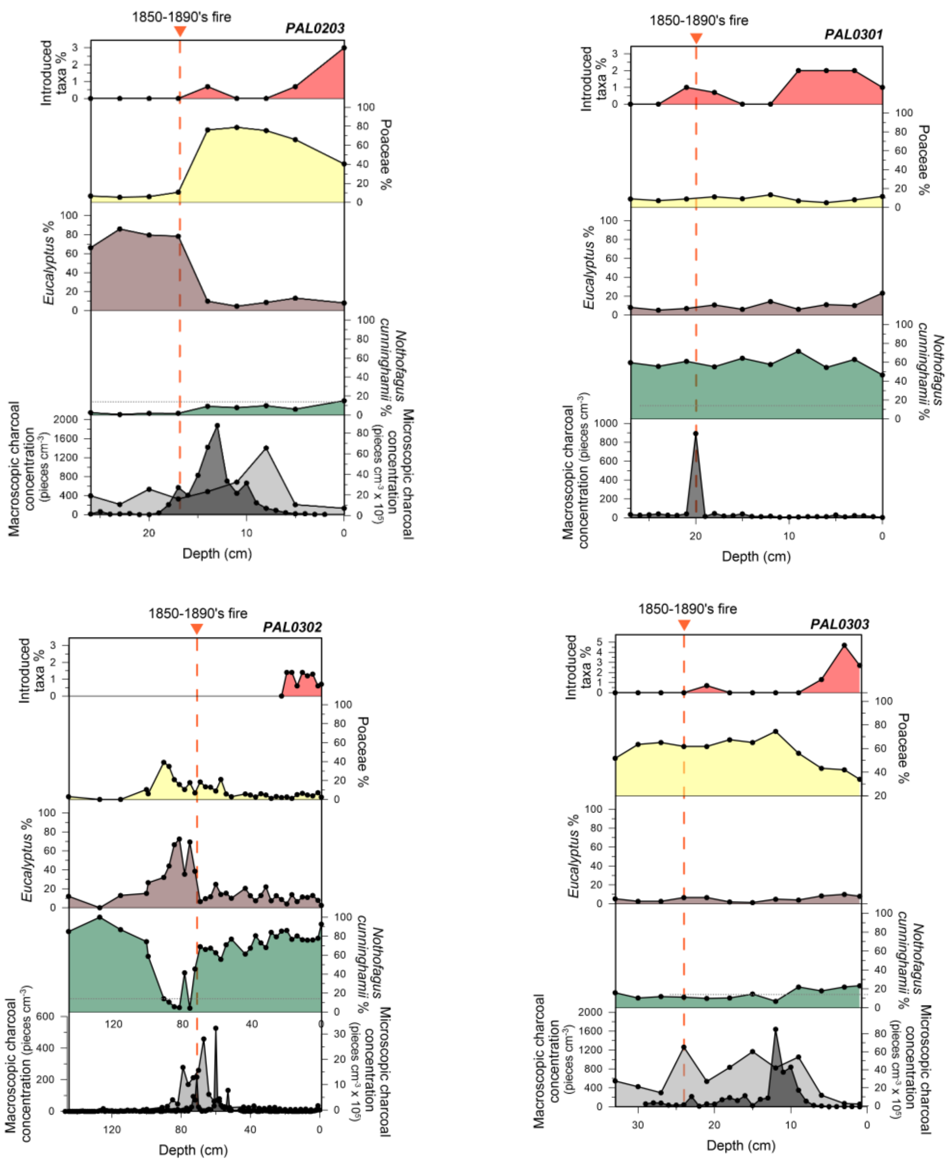

Table S2: Results of two-sample t-tests. 'Shielded loggers only' subset includes E009, L012, S-Trap017, W003 and W018 (See Figure 1b in main text for site locations).

Dataset	Loggers included	Variable	p value
Full dataset	Shielded loggers only	Temperature	0.312
NDJFM subset	Shielded loggers only	Temperature	0.349
Full dataset	Shielded loggers only	Humidity	2.18E-09
NDJFM subset	Shielded loggers only	Humidity	9.42E-09

Table S3: Archaeological sites used in the calculation of human activity estimates (human population dynamics) (GR_{Ann}). Data sourced from SahulArch Radiocarbon collection on the OCTOPUS v.2 database (Saktura et al. 2021). Site locations in SahulArch are obfuscated within a 25 km radius using a randomising algorithm that only represent a possible site location. The non-obfuscated site coordinates are still stored in relational attribute tables but are not made public. Only sites from within the 'King', 'Tasmanian Central Highlands', 'Tasmania West' and 'Tasmanian Northern Slopes' Interim Biogeographic Regionalisation for Australia (IBRA) were chosen for this study (see Figure S1).

Site Name	Site Type	Long	Lat	IBRA Region	Material dated	14C age	14C error	Calibrated Age (median)	Bin age
Trial Harbour	Shell midden	145.38	-42.0	Tasmanian West	Charcoal	215	95	192	200
Arthur River	Shell midden	144.67	-41.1	King	Charred	310	78	328	400
Overhang Cave	Rockshelter or cave	146.02	-42.0	Tasmanian Central Highlands	Charcoal	330	105	337	400
Toolumbunner	Quarry	146.42	-41.5	Tasmanian Northern Slopes	Charcoal	330	70	366	400
Overhang Cave	Rockshelter or cave	146.02	-42.0	Tasmanian Central Highlands	Charcoal	340	105	349	400
Toolumbunner	Quarry	146.42	-41.5	Tasmanian Northern Slopes	Charcoal	370	25	390	400
Toolumbunner	Quarry	146.42	-41.5	Tasmanian Northern Slopes	Charcoal	400	25	418	600
Warragarra Rockshelter	Rockshelter or cave	146.46	-41.7	Tasmanian Central Highlands	Bone	410	60	412	600
Arthur River	Shell midden	144.67	-41.1	King	Charred	420	70	418	600
Cataraqui Monument quarry	Quarry	143.86	-40.1	King	Charcoal	450	105	434	600
King River Valley 3	Open site	145.85	-42.2	Tasmanian Central Highlands	Charcoal	460	60	465	600
Cataraqui Point	Shell midden	143.86	-40.1	King	Charcoal	475	70	472	600
Toolumbunner	Quarry	146.42	-41.5	Tasmanian Northern Slopes	Charcoal	480	80	472	600
Cave Bay Cave	Rockshelter or cave	144.45	-40.3	King	Charcoal	700	90	620	800
Cave Bay Cave	Rockshelter or cave	144.45	-40.3	King	Charcoal	760	70	660	800
Cave Bay Cave	Rockshelter or cave	144.45	-40.3	King	Charcoal	770	87	669	800

Parmerpar Meethaner	Rockshelter or cave	146.08	-41.7	Tasmanian Northern Slopes	Charcoal	780	50	676	800
Cave Bay Cave	Rockshelter or cave	144.45	-40.3	King	Charcoal	840	100	730	1000
Cave Bay Cave	Rockshelter or cave	144.45	-40.3	King	Charcoal	840	100	730	1000
Cave Bay Cave	Rockshelter or cave	144.45	-40.3	King	Charcoal	870	70	747	1000
Cave Bay Cave	Rockshelter or cave	144.45	-40.3	King	Charcoal	900	90	779	1000
Cave Bay Cave	Rockshelter or cave	144.45	-40.3	King	Charcoal	900	250	812	1000
Cave Bay Cave	Rockshelter or cave	144.45	-40.3	King	Charcoal	935	70	807	1000
Cave Bay Cave	Rockshelter or cave	144.45	-40.3	King	Charcoal	990	90	851	1000
Cave Bay Cave	Rockshelter or cave	144.45	-40.3	King	Charcoal	1000	60	855	1200
Cave Bay Cave	Rockshelter or cave	144.45	-40.3	King	Charcoal	1070	110	932	1200
Cape Sorrell	Shell midden	145.38	-42.1	Tasmanian West	Charcoal	1120	70	987	1200
Cave Bay Cave	Rockshelter or cave	144.45	-40.3	King	Charcoal	1230	80	1101	1400
Cliff Cave	Rockshelter or cave	143.90	-40.1	King	Charcoal	1330	80	1196	1400
Green's Creek	Shell midden	144.69	-41.2	King	Charcoal	1330	80	1196	1400
Green's Creek	Shell midden	144.69	-41.2	King	Charcoal	1350	200	1206	1400
Little Duck Bay	Shell midden	145.10	-40.8	King	Charcoal	1370	70	1229	1400
Little Duck Bay	Shell midden	145.10	-40.8	King	Charcoal	1500	150	1367	1600
Mount Cameron West	Shell midden	144.71	-40.9	King	Charcoal	1560	70	1412	1600
Nelson River Karst	Open site	145.96	-42.2	Tasmanian Central Highlands	Charcoal	1580	130	1447	1600
Mount Cameron West	Shell midden	144.71	-40.9	King	Charcoal	1610	160	1480	1800
PH90/1	Rockshelter or cave	145.69	-42.5	Tasmanian West	Charcoal	1720	100	1584	1800

Mount Cameron West	Shell midden	144.71	-40.9	King	Charcoal	1760	120	1632	1800
Mount Cameron West	Shell midden	144.71	-40.9	King	Charcoal	1800	90	1673	2000
Mount Cameron West	Shell midden	144.71	-40.9	King	Charcoal	1850	80	1733	2000
Mount Cameron West	Shell midden	144.71	-40.9	King	Charcoal	1885	125	1774	2000
Mount Cameron West	Shell midden	144.71	-40.9	King	Charcoal	2025	85	1936	2000
Mt Cameron West	Burial (human)	144.71	-40.9	King	Charcoal	2185	100	2126	2200
Parmerpar Meethaner	Rockshelter or cave	146.08	-41.7	Tasmanian Northern Slopes	Charcoal	2210	50	2162	2200
Muttonbird Midden	Shell midden	144.73	-40.3	King	Charcoal	2350	150	2342	2400
Muttonbird Midden	Shell midden	144.73	-40.3	King	Charcoal	2420	60	2441	2600

Figure S2: (A) Map of Australia, black square indicates Tasmania; **(B)** Tasmania overlain by average annual rainfall isohyets showing the orographic rainfall gradient across the island (Land Tasmania 2022) and location of our study region (yellow star), archaeological sites (red squares) selected for human demography calculation and Tasmanian sites (grey triangles) used in paleofire analysis: Western Tasmania charcoal influx curve calculated using the *R* package *paleofire* v.1.2.4 (Blarquez et al. 2014) updated to SHCal20 (Hogg et al. 2020) from sites outlined in Supplementary Information Figure S2 and Table S4 (site data derived from Mariani and Fletcher 2017). Grey areas with hatching indicate the 'King', 'Tasmanian Central Highlands', 'Tasmania West' and 'Tasmanian Northern Slopes' Interim Biogeographic Regionalisation for Australia (IBRA) regions.

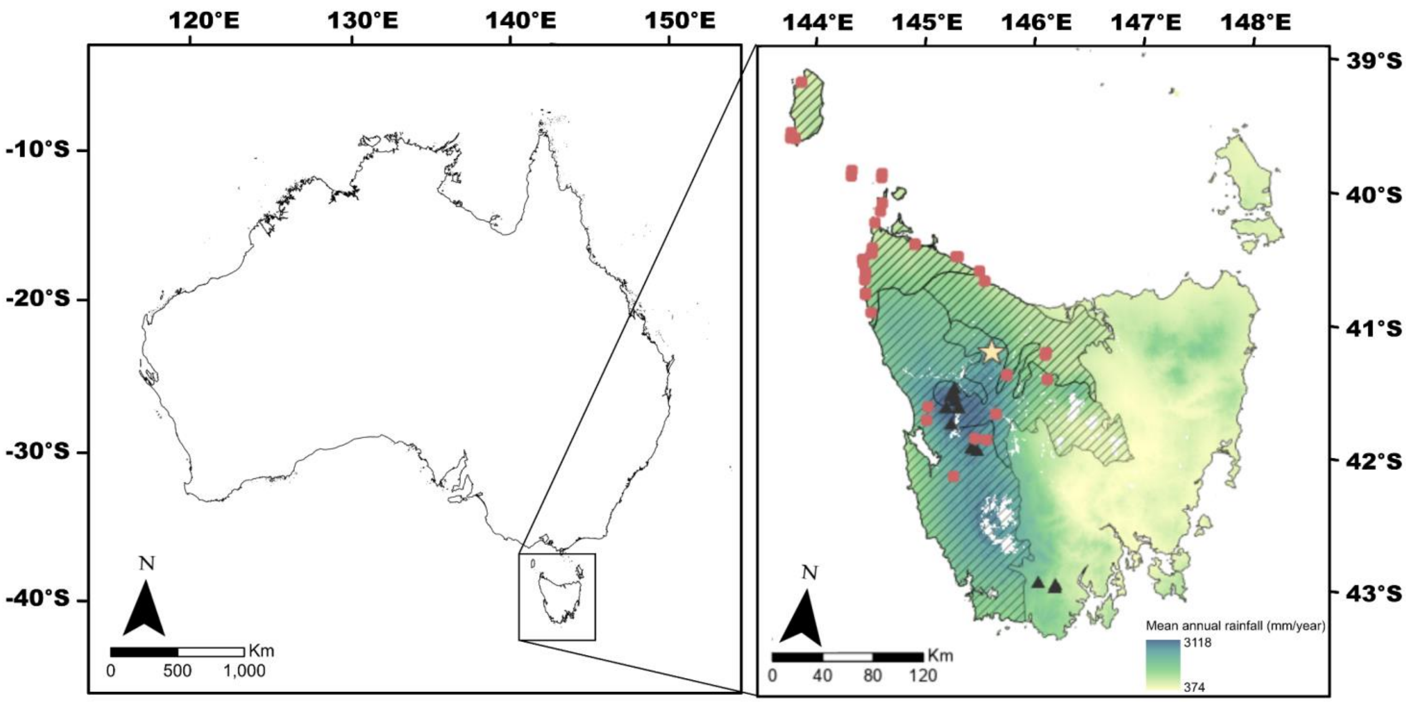

Table S4: List of sites in western Tasmania used for the paleofire analysis (Mariani and Fletcher 2017).

Core code	Site name	Latitude	Longitude	Elevation (m a.s.l.)	Maximum basin depth (m)	Maximum age of the record (yrs bp)	Number of ^{14}c dates	^{210}pb chronology
TAS1102	Gaye	41°49′35.12″S	145°36′11.99″E	892	1.2	9933	4	N
TAS1104	Basin	41°58′50.96″S	145°32′53.84″E	577	5.2	20749	10	Y
TAS1106	Gwendolyn	42°15′44.58″S	145°49′23.11″E	923	30	11452	8	Y
TAS1107	Nancy	42°15′31.56″S	145°49′37.62″E	1037	24.1	11272	7	Y
TAS1108	Vera	42°16′28.53″S	145°52′47.73″E	571	48	18105	11	Y
TAS1110	Osborne	43°12′58.37″S	146°45′33.46″E	920	9.5	13899	11	Y
TAS1203	Julia	41°53′21.22″S	145°34′34.09″E	616	12	10113	4	N
TAS1205	Square tarn	43°12′51.52″S	146°35′39.19″E	865	3.5	7958	5	Y
TAS1207	Hartz	43°14′17.12″S	146°45′23.62″E	952	40.5	5207	5	N
TAS1402	Selina	41°52′39.80″S	145°36′34.01″E	516	7.4	17265	15	N
TAS1501	Owen tarn	42°5′58.6″S	145°36′33.95″E	969	7	7442	11	Y
TAS1503	Isla	41°58′13.91″S	145°39′55.57″E	720	14	11786	9	Y
TAS1504	Rolleston	41°55′17.35″S	145°37′29.12″E	560	42	4488	7	N

Figure S3: **(A)** Histogram (50-year bins) of the ^{14}C errors for all archaeological dates from Table S3 derived from the OCTOPUS database (grey bars) and their cumulative probabilities. **(B)** Histograms (200-year bins) of all calibrated archaeological dates from Table S3 derived from the OCTOPUS database (Saktura et al. 2021) (grey bars, background, *n* = 49) and all calibrated archaeological dates with ^{14}C errors less than 100 years (white bars, foreground, *n* = 37).

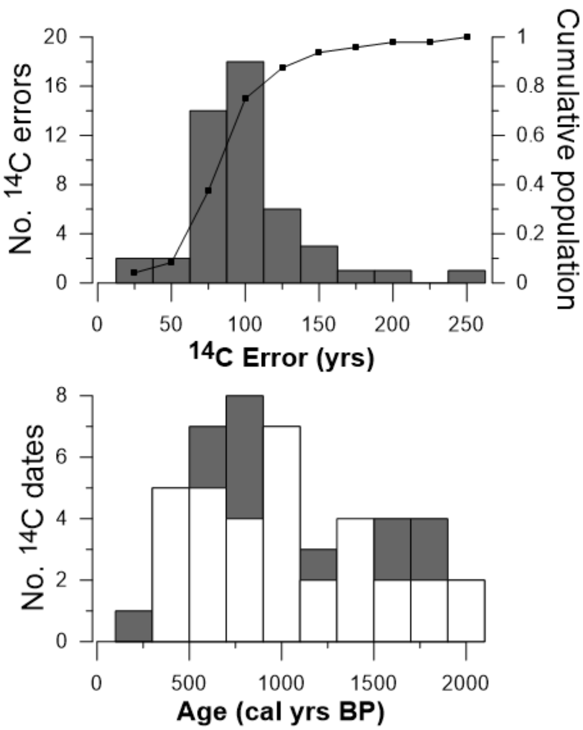

Supplementary Information Text

There has been substantial criticism of such approaches to human demography estimates, with questions raised as to whether fluctuations in the density of radiocarbon dates reflect changes in human demography and the ‘dates as data’ approach, whilst also using radiocarbon dates have their own specific statistical challenges (e.g., sampling error and errors produced in calibration) (Becerra-Valdivia et al. 2020, Blackwell and Buck 2003, Carleton 2021, Contreras and Meadows 2014, Hiscock and Attenbrow 2016, Rick 1987, Torfing 2015).

To overcome the above issues, summed probability distribution (SPD) and composite kernel density estimates (CKDE) of calibrated radiocarbon dates have instead been utilised to understand human demography via radiocarbon dates (Bevan et al. 2017, Contreras and Meadows 2014, Crema et al. 2016, Crema and Shoda 2021, Friman and Lagerås 2022, Kerr and McCormick 2014, Ramsey 2017, Shennan et al. 2013, Timpson et al. 2014). The approach of SPDs assumes that there is a positive (but not necessarily linear) relationship between the number of radiocarbon dates and population size (as radiocarbon dates are derived from archaeological features, and that the number of dates is high) (Contreras and Meadows 2014, Crema and Shoda 2021, Friman and Lagerås 2022). Despite the wide use of SPDs, these approaches also tend to ignore the issue of sampling error and calibration effects (Crema et al. 2016, Ramsey 2017). Recently there have been attempts to address these via: (1) bootstrapping (sampling errors); (2) moving window (calibration effects); (3) Monte-Carlo simulation or random permutation techniques (null hypothesis significance testing) (Crema et al. 2016, Shennan et al. 2013, Timpson et al. 2014); (4) fitting Bayesian non-parametric models (to reconstruct the ‘shape’ of the probability distribution of radiocarbon dates) (Price et al. 2020, Ramsey 2017); (5) conventional statistical methods on SPDs (e.g., correlation and regression analyses) (Fernández-López de Pablo et al. 2019, Kelly et al. 2013, Lima et al. 2020, Palmisano et al. 2017, Riris and Arroyo-Kalin 2019) and; (6) flexible family of bounded growth models (where discrete time windows are fitted via Markov

Chain Monte-Carlo (MCMC) and compared using the Widely Applicable Information Criterion (WAIC)) (Crema and Shoda 2021). However, these all come with their own advantages and limitations (discussed within referenced studies). Chiefly for this paper, using SPDs tend to require a minimum sample size of 500 radiocarbon dates (e.g., Bevan et al. 2017, Contreras and Meadows 2014, Crema et al. 2016, Crema and Shoda 2021, Kerr and McCormick 2014, Ramsey 2017, Shennan et al. 2013, Timpson et al. 2014); our study is 49 radiocarbon dates and there are only 301 for Tasmania on the OCTOPUS database – once marine shells and erroneous dates are removed (Ramsey 2017, Saktura et al. 2021, Williams 2012). Studies highlight that for complex models a high number of radiocarbon dates are required to produce reliable results (pointing to the intensity of archaeological research in those regions that utilise these techniques), with small sample sizes resulting in incorrect inferences, large higher posterior density intervals, noise from limited samples and calibration process and excessive spread resulting from measurement uncertainty (Crema 2022, Crema et al. 2016, Ramsey 2017). In this paper we acknowledge the limitations of using a small dataset and the inability to successfully run more current approaches to human demography. However, we shift our interpretation away from "population size" and towards shifts between localised and dispersed patterns of care for Country and intensity of occupation.

Commented [MF1]: This is good. The above is possibly over long, over technical and over apologetic - perhaps shift this to the supp info and keep what we did and what we think it means in the manuscript? That way we show that we have considered these things and we are going with the best of what we have.

Supplementary Information References

Becerra-Valdivia, L., R. Leal-Cervantes, R. Wood and T. Higham 2020. "Challenges in sample processing within radiocarbon dating and their impact in 14c-dates-as-data studies." Journal of Archaeological Science **113**: 105043.

Bevan, A., S. Colledge, D. Fuller, R. Fyfe, S. Shennan and C. Stevens 2017. "Holocene fluctuations in human population demonstrate repeated links to food production and climate." Proceedings of the National Academy of Sciences **114**(49): E10524-E10531.

Blackwell, P. G. and C. E. Buck 2003. "The late glacial human reoccupation of north-western europe: New approaches to space-time modelling." Antiquity **77**(296): 232-240.

Carleton, W. C. 2021. "Evaluating bayesian radiocarbon-dated event count (rec) models for the study of long-term human and environmental processes." Journal of Quaternary Science **36**(1): 110-123.

Contreras, D. A. and J. Meadows 2014. "Summed radiocarbon calibrations as a population proxy: A critical evaluation using a realistic simulation approach." Journal of Archaeological Science **52**: 591-608.

Crema, E. R. 2022. "Statistical inference of prehistoric demography from frequency distributions of radiocarbon dates: A review and a guide for the perplexed." Journal of Archaeological Method and Theory **29**(4): 1387-1418.

Crema, E. R., J. Habu, K. Kobayashi and M. Madella 2016. "Summed probability distribution of 14c dates suggests regional divergences in the population dynamics of the jomon period in eastern japan." PloS one **11**(4): e0154809.

Crema, E. R. and S. Shoda 2021. "A bayesian approach for fitting and comparing demographic growth models of radiocarbon dates: A case study on the jomon-yayoi transition in kyushu (japan)." PLoS One **16**(5): e0251695.

Fernández-López de Pablo, J., M. Gutiérrez-Roig, M. Gómez-Puche, R. McLaughlin, F. Silva and S. Lozano 2019. "Palaeodemographic modelling supports a population bottleneck during the pleistocene-holocene transition in iberia." Nature communications **10**(1): 1872.

Friman, B. and P. Lagerås 2022. "From neolithic boom-and-bust to iron age peak and decline: Population and settlement dynamics in southern sweden inferred from summed radiocarbon dates." European Journal of Archaeology: 1-21.

Hiscock, P. and V. Attenbrow 2016. "Dates and demography? The need for caution in using radiometric dates as a robust proxy for prehistoric population change." Archaeology in Oceania **51**(3): 218-219.

Kelly, R. L., T. A. Surovell, B. N. Shuman and G. M. Smith 2013. "A continuous climatic impact on holocene human population in the rocky mountains." Proceedings of the National Academy of Sciences **110**(2): 443-447.

Kerr, T. R. and F. McCormick 2014. "Statistics, sunspots and settlement: Influences on sum of probability curves." Journal of Archaeological Science **41**: 493-501.

Land Tasmania. 2022). "Land information system tasmania (list) data." Retrieved 5th May, 2023, from https://listdata.thelist.tas.gov.au/opendata/.

Lima, M., E. M. Gayo, C. Latorre, C. M. Santoro, S. A. Estay, N. Cañellas-Boltà, O. Margalef, S. Giralt, A. Sáez and S. Pla-Rabes 2020. "Ecology of the collapse of rapa nui society." Proceedings of the Royal Society B **287**(1929): 20200662.

Mariani, M. and M.-S. Fletcher 2017. "Long-term climate dynamics in the extra-tropics of the south pacific revealed from sedimentary charcoal analysis." Quaternary Science Reviews **173**: 181-192.

Marsden-Smedley, J. B. 1998. Changes in southwestern tasmanian fire regimes since the early 1800s. Papers and proceedings of the Royal Society of Tasmania.

Palmisano, A., A. Bevan and S. Shennan 2017. "Comparing archaeological proxies for long-term population patterns: An example from central italy." Journal of Archaeological Science **87**: 59-72.

Price, M. H., J. M. Capriles, J. A. Hoggarth, K. Bocinsky, C. E. Ebert and J. H. Jones 2020. "End-to-end bayesian analysis of 14c dates reveals new insights into lowland maya demography." bioRxiv: 2020.2007. 2002.185256.

Ramsey, C. B. 2017. "Methods for summarizing radiocarbon datasets." Radiocarbon **59**(6): 1809-1833.

Rick, J. W. 1987. "Dates as data: An examination of the peruvian preceramic radiocarbon record." American Antiquity **52**(1): 55-73.

Riris, P. and M. Arroyo-Kalin 2019. "Widespread population decline in south america correlates with mid-holocene climate change." Scientific reports **9**(1): 6850.

Saktura, W. M., H. Munack, A. T. Codilean, R. Wood, F. Petchey, Z. Jacobs, A. Williams and S. Ulm 2021. "Octopus database v. 2: The sahularch radiocarbon collection."

Shennan, S., S. S. Downey, A. Timpson, K. Edinborough, S. Colledge, T. Kerig, K. Manning and M. G. Thomas 2013. "Regional population collapse followed initial agriculture booms in mid-holocene europe." Nature communications **4**(1): 2486.

Timpson, A., S. Colledge, E. Crema, K. Edinborough, T. Kerig, K. Manning, M. G. Thomas and S. Shennan 2014. "Reconstructing regional population fluctuations in the european neolithic using radiocarbon dates: A new case-study using an improved method." Journal of Archaeological Science **52**: 549-557.

Torfing, T. 2015. "Layers of assumptions: A reply to timpson, manning, and shennan." Journal of archaeological science **63**: 203-205.

Williams, A. N. 2012. "The use of summed radiocarbon probability distributions in archaeology: A review of methods." Journal of Archaeological Science **39**(3): 578-589.